Hindawi
Journal of Nanotechnology
Volume 2023, Article ID 2381623, 7 pages
https://doi.org/10.1155/2023/2381623

Research Article

Synthesis and Properties of Magnetic-Luminescent Fe_3O_4@ZnO/C Nanocomposites

Astuti,[1] **Syukri Arief**,[2] **Muldarisnur**,[1] **Zulhadjri**,[2] **and R. A. Usna**[1]

[1]*Physics Department, Andalas University, Padang, West Sumatra, Indonesia*
[2]*Chemistry Department, Andalas University, Padang, West Sumatra, Indonesia*

Correspondence should be addressed to Syukri Arief; syukriarief@sci.unand.ac.id

Received 5 October 2022; Revised 18 March 2023; Accepted 29 March 2023; Published 8 April 2023

Academic Editor: Mozhgan Afshari

A Fe_3O_4@ZnO/C nanocomposite with a core-shell structure was synthesized using the co-precipitation method. To prevent the aggregation of the Fe_3O_4 magnetic particles, polyethylene glycol (PEG) was added. The X-ray diffractometer (XRD) results confirmed the formation of Fe_3O_4 and ZnO phases, with Fe_3O_4 having a cubic crystal system and ZnO having a hexagonal crystal system. Carbon in Fe_3O_4@ZnO/C had no effect on the crystal structure of Fe_3O_4@ZnO. Images from transmission electron microscopy (TEM) and scanning electron microscopy (SEM) revealed that the nanocomposite formed a core-shell structure. The Fourier transform infrared (FTIR) spectra verified the presence of bonds among ZnO, Fe_3O_4, and carbon. The appearance of the stretching vibration of the C≡C bond on the Fe_3O_4@ZnO/C sample revealed the nanocomposites' carbon coupling. Photoluminescence (PL) spectroscopy was used to characterize the optical properties of the nanocomposites. Based on the results of the PL, the sample absorption of visible light was in the wavelength range of 400–700 nm. The photoluminescence of Fe_3O_4@ZnO differed from that of the Fe_3O_4@ZnO/C, especially in the deep-level emission (DLE) band. There was a phenomenon of broadening and shift of the band at a shorter wavelength, namely, in the blue wavelength region. Magnetic properties were characterized by vibrating-sample magnetometry (VSM). Based on the VSM results, the sample coupled with carbon exhibited a decrease in magnetic saturation. The presence of carbon changed photon energy into thermal energy. So, this material, apart from being a bioimaging material, can also be developed as a photothermal therapy material.

1. Introduction

Fe_3O_4 nanoparticles are considered a potential candidate for application as magnetic bioimaging materials, by making Fe_3O_4 nanoparticles covered by biocompatible materials [1–3]. Magnetic nanoparticles made of Fe_3O_4 have a high surface-to-volume ratio and a high surface energy. As a result, the magnetic nanoparticles tend to agglomerate to reduce the surface energy. In addition, these nanoparticles are highly reactive and easily oxidized which decrease their magnetic properties and dispersibility. Various strategies are further being developed by researchers to solve these problems. These strategies include doping Fe_3O_4 and surface coating of magnetic nanoparticles with organic molecules (such as surfactants, polymers, and biomolecules) or non-organic materials (such as SiO_2 and Au). The coating material for magnetic nanoparticles must be compatible and maintain the stability of the magnetic nanoparticles [4–6]. Several coating materials for Fe_3O_4 have been proposed, including polymers (such as dextran, albumin, polyethylene glycol, polyvinylpyrrolidone [7], folic acid [8, 9], chitosan [10], and silica [11]).

Combining magnetic and luminescent materials, such as lanthanide [12, 13], carbon/graphene [14, 15], and semiconductor [16, 17], produces materials with unique properties for different applications. Several researchers combined Fe_3O_4@ZnO nanocomposites with other materials to be utilized for antibacterial application [16], photodegradation of organic pollutants [18], and targeted drug delivery [19]. However, only a few studies have developed Fe_3O_4@ZnO nanocomposites as bioimaging materials. The main advantage of such nanocomposites for biological

applications is nontoxicity and biocompatibility. The surface modification must not significantly change the biocompatibility, photoluminescence, and magnetic properties. One of the materials that can be employed as a combiner for Fe_3O_4@ZnO is carbon. Carbon can also transfer the generated heat by the electron recombination process on the ZnO surface. Therefore, this material has multiple functions in biological applications, such as bioimaging and photothermal therapy of cancerous cells [20, 21].

In this study, a class of multifunctional nanocomposites is presented that combines superparamagnetic Fe_3O_4, ZnO, and surface modification of Fe_3O_4@ZnO with carbon. Fe_3O_4@ZnO/C is the core-shell structure of Fe_3O_4-based nanocomposite materials. The co-precipitation method was used to create a Fe_3O_4@ZnO nanocomposite. To prevent Fe_3O_4 agglomeration, polyethylene glycol (PEG) was used as a coating material. The carbon shell acted as a protective shell making it stable, free from external environmental influence, and biocompatible. XRD (Bruker D8 Advance) was utilized to determine the phase and crystal structure. The qualitative phase analysis of the XRD characterization's diffraction pattern will be compared to established crystallographic databases, including the International Center for Diffraction Data (ICDD). To investigate optical properties, photoluminescence (PL, Horiba MicO Photoluminescence Microspectrometer) was used. SEM (SU3500) and TEM (FEI Tecnai G2 20 S-Twin) were used to examine the morphology and particle size of the samples. The chemical bonds formed were determined using FTIR (FTIR, Nicolet iS50 FTIR). In addition VSM (VSM250) was used to examine the magnetic properties of materials, which were then represented as a hysteresis curve.

2. Materials and Methods

2.1. Synthesis of Fe_3O_4@ZnO Nanocomposites. The synthesis of nanocomposite Fe_3O_4@ZnO/C begins with the synthesis of Fe3O4 nanoparticle combined with ZnO by the co-precipitation method [12, 22, 23]. A modified co-precipitation method was used to create Fe_3O_4@ZnO nanoparticles as done by Astuti et al. [24].

2.2. Synthesis of Fe_3O_4@ZnO/C Nanocomposites. In 25 mL of distilled water, 2 g of PEG was dissolved. Following that, 1 g of glucose was added, stirred for 30 minutes, heated in an oven at 300°C for 1 hour, and then dissolved in 10 mL of distilled water. Fe_3O_4@ZnO (0.1 g) and 5 mL of carbon solution were mixed, stirred, and then heated in the furnace at 250°C. The resulting powder was named Fe_3O_4@ZnO/C nanocomposite.

3. Results and Discussion

XRD analyzed the crystal structure, phase, and purity of the nanomaterials (Figure 1). Measurement results for Fe_3O_4 match the ICDD code 01-071-6339. Fe_3O_4 lattice parameters were $a = b = c = 8.3153$ Å, according the cubic system of Fe_3O_4 nanoparticles. The crystalline peaks of Fe_3O_4 observed at 2θ values of 30.4593°, 35.7909°, 43.3784°, 53.9629°, 57.3681°, 63.2529°, and 90.5352° can be assigned to the planes with Miller indices of (220), (311), (400), (422), (511), (440), and (731).

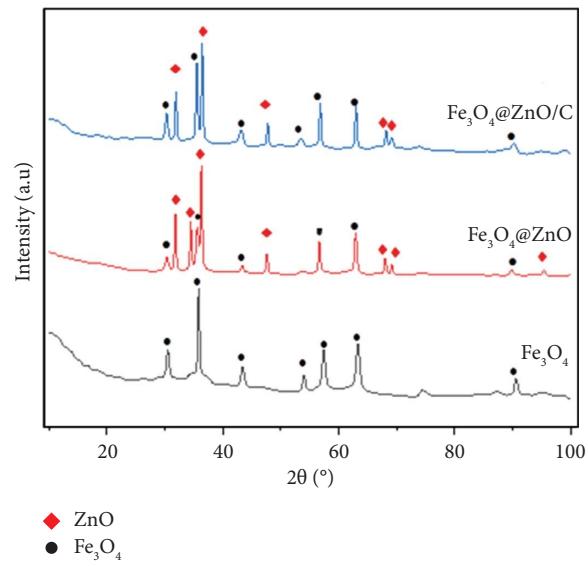

Figure 1: XRD patterns of Fe_3O_4 and nanocomposites.

Fe_3O_4 and ZnO were present in the Fe_3O_4@ZnO sample, and they had simple cubic and hexagonal wurtzite crystalline structures, respectively. The Fe_3O_4 phase had a cubic crystal structure with lattice parameters of $a = b = c = 8.3761$ Å, according to the ICDD code 01-076-7171. ZnO crystal structure has lattice parameters of $a = 3.2525$ Å, $b = 3.2525$ Å, and $c = 5.2111$ Å and is depicted in ICDD 01-075-7917. The crystalline ZnO peaks were observed at the 2θ values of 31.7748°, 34.4273°, 36.2561°, 47.5718°, 67.9733°, 69.1152°, and 95.3214° which can be, respectively, assigned to the planes with Miler indices of (100), (002), (101), (102), (112), (201), and (211). The formation of the core-shell structure of Fe_3O_4@ZnO can be seen from the emergence of peaks (311) in Fe_3O_4 and (101) in ZnO, while the sample Fe_3O_4@ZnO/C showed similar peaks and crystal structure to Fe_3O_4@ZnO. This result shows that the presence of carbon has no effect on the crystal structure of Fe_3O_4@ZnO. The FTIR results confirm XRD measurements, indicating the presence of carbon in the Fe_3O_4@ZnO/C nanocomposite.

Figure 2 shows the results of FTIR measurements in the wavenumber range of 400–4000 cm^{-1}. Several absorption peaks in the sample Fe_3O_4@ZnO were observed, namely, the wavenumber 3352.34 cm^{-1} related to the vibration of the -OH (hydroxyl) group. The absorption peaks illustrated the formation of PEG in the C-O and C-C vibrations of the sample, namely, at 1247.00 cm^{-1}, 1087.87 cm^{-1}, and 940.31 cm^{-1}. There were vibrations of tetrahedral Fe-O and octahedral Fe-O bonds at wavenumbers of 545.86 cm^{-1} and 484.14 cm^{-1}, respectively, and Zn-O bonds at 424.35 cm^{-1} [25]. Apart from the same absorption peaks, Fe-O, Zn-O, C-H, and C-O, no differences were found in the Fe_3O_4@ZnO/C sample. However, no absorption peak was found in the Fe_3O_4@ZnO sample, namely, the C≡C bond. Wavenumbers of 2086.05 cm^{-1} and 2860.48 cm^{-1} indicated C≡C bonds and

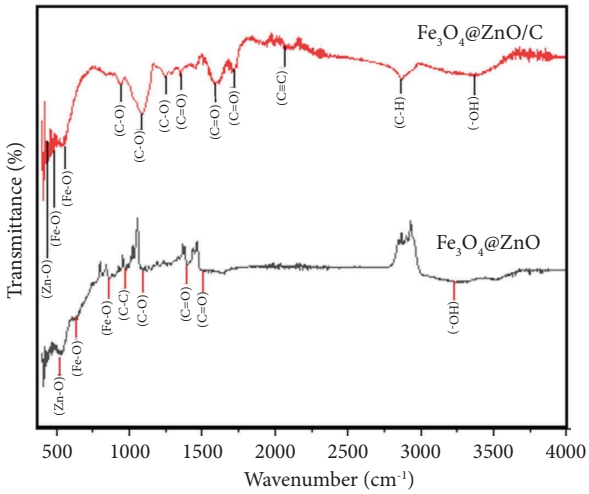

FIGURE 2: FTIR spectra of Fe_3O_4@ZnO and Fe_3O_4@ZnO/C nanocomposites.

C-H bonds formed in the sample, respectively. The absorption peaks at wavenumbers of 1713.78 cm^{-1}, 1599.98 cm^{-1}, and 1348.27 cm^{-1} corresponded to bond stretching vibrations (C=O). The appearance of the stretching vibration of the C≡C bond on the Fe_3O_4@ZnO/C sample resulted from carbon demonstrating the sample coupling with carbon. Besides, a more substantial shift and enhancement of absorption peaks of Fe_3O_4@ZnO/C were detected compared to Fe_3O_4@ZnO which can be possibly due to the bond between the C and O atoms in ZnO or Fe_3O_4. This result shows that the synthesis of Fe_3O_4@ZnO/C using the co-precipitation method was successful.

As shown in Figure 3(a), TEM characterization was performed to determine the core-shell structure of the sample represented by Fe_3O_4@ZnO. The morphology of Fe_3O_4 nanoparticles depicts a spherical shape with an approximate size of 15 nm. These clusters resemble a chain-like structure due to magnetic dipole interactions between nearby Fe_3O_4 particles. Based on Figure 3(a), it can be seen clearly that the black Fe_3O_4 is coated by the gray ZnO, which confirms the core-shell structure of the sample. These results were also in good agreement with the literature [17, 26]. Figure 3(b) shows a TEM image of the Fe_3O_4@ZnO/C nanocomposite. Based on the analysis of the diffraction pattern, it was found that Fe_3O_4 and ZnO, had a particle size of less than 20 nm, while carbon was in the form of nanorods composed of Fe_3O_4@ZnO particles.

The SEM images of the Fe_3O_4@ZnO sample demonstrate aggregated spherical particles with sizes ranging from 50 to 100 nm (Figure 4), which can be distinguished from the white color assigned to ZnO nanoparticles covering the Fe_3O_4 particles. In the preparation steps, the dispersion of Fe_3O_4 in Zn^{2+} can lead to the adsorption of Zn^{2+} ions on the Fe_3O_4 surface. The growth of this bound ZnO nanoparticle can be caused by Zn^{2+} ions from nearby Fe_3O_4 surfaces and the freely available Zn^{2+} ions. This can also result in the attachment of a specific portion of every ZnO particle to the Fe_3O_4 particles.

PL spectroscopy and VSM were used to investigate the room-temperature luminescence and magnetic properties, respectively. The PL spectrum of Fe_3O_4@ZnO (Figure 5) shows a UV emission peak at 381.86 nm for Fe_3O_4@ZnO and 382.49 nm for Fe_3O_4@ZnO/C, as well as a broad visible emission peak ranging from 400 to 800 nm. The visible photoluminescence emission centers in the Fe_3O_4@ZnO sample are determined by ZnO vacancies and surface defects. Although the PL mechanism of the visible ZnO band is unknown, a photoluminescence mechanism can be proposed. According to Figure 5, emissions in the 400 nm to 800 nm range are commonly referred to as "deep-level emissions" (DLEs). The DLE is caused by levels allowed inside the ZnO band gap. Transitions with energy in the visible range of the spectrum are produced by the allowed levels. The band broadness presumably resulted from a superposition of many different deep levels (yellow peak, green peak, and blue peak) emitting simultaneously [27, 28]. The presence of a strong and broad emission peak in the visible region indicates that ZnO has a higher concentration of defects. The most common surface defects reported in ZnO are oxygen vacancies, and the intensity of the green emission depends on the concentration of the oxygen vacancies. The difference between the DLE of Fe_3O_4@ZnO and Fe_3O_4@ZnO/C is visible. There is a broadening of the DLE band in Fe_3O_4@ZnO/C, and there is a shift in the band to a shorter wavelength, namely, in the blue wavelength region caused by the presence of carbon atoms. Carbon has two significant peaks at 450 nm and 510 nm attributing to the sp^2 domain's π-$\pi*$ transition and the n-$\pi*$ transition of the surface functional group, respectively. Interstitial oxygen cause yellow emission in ZnO which can be reduced by the presence of C atoms resulting in a shift in the blue region emission. The green and yellow peaks were observed in the Fe_3O_4@ZnO sample. Besides, the blue shift was observed in the Fe_3O_4@ZnO/C sample. Free exciton (FE) emissions dominated the UV emission band which is generally ascribed to the band-to-band transition.

Furthermore, a slight decrease in the intensity of photoluminescence of the Fe_3O_4@ZnO/C sample was identified compared to that of the sample Fe_3O_4@ZnO. A reduction in the intensity of the Fe_3O_4@ZnO/C photoluminescence is closely related to the recombination of the electron-hole pairs. It can be concluded that the weaker the PL intensity, the slower the recombination of photogenerated electron-hole pairs.

The results of measuring the magnetic properties of Fe_3O_4, Fe_3O_4@ZnO, and Fe_3O_4@ZnO/C nanocomposites are shown in Figure 6. The coercivity values (H_c) of Fe_3O_4, Fe_3O_4@ZnO, and Fe_3O_4@ZnO/C were calculated as 0.0031 T, 0.0037 T, and 0.0038 T, respectively, while the saturation magnetization (M_s) values were different, as shown in Table 1.

Based on Table 1 and Figure 6, the M_s value of Fe_3O_4 nanoparticles is 68.10 emu/g. It decreased to 66.53 emu/g for the Fe_3O_4@ZnO sample. The decrease in M_s value of the Fe_3O_4@ZnO nanocomposite was due to the addition of nonmagnetic PEG and ZnO and also the presence of oxygen-containing groups in the matrix of Fe_3O_4

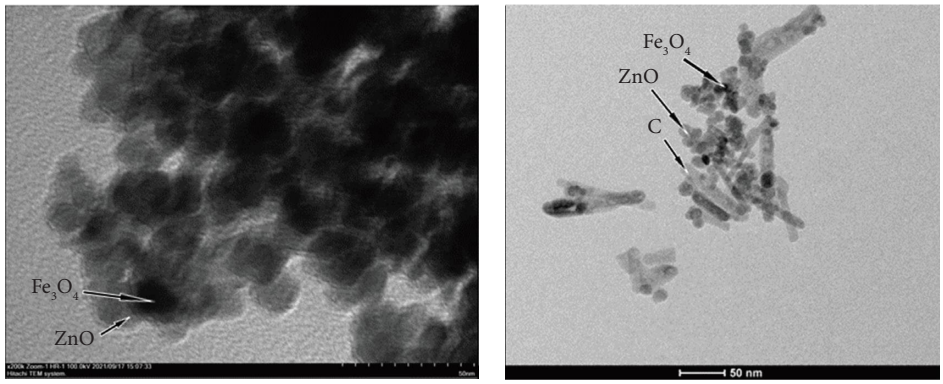

(a) (b)

Figure 3: TEM image of (a) Fe_3O_4@ZnO and (b) Fe_3O_4@ZnO/C nanocomposites.

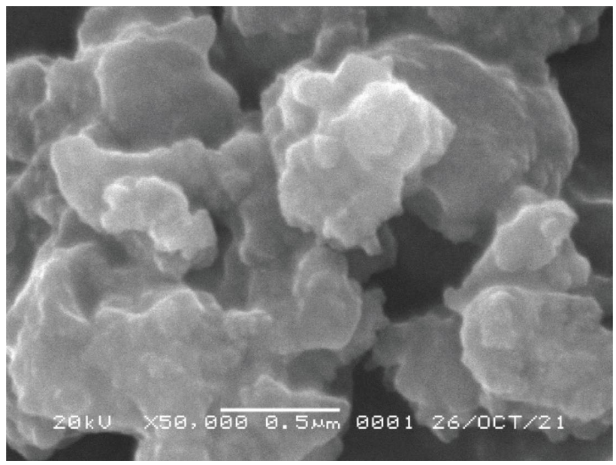

Figure 4: SEM image of Fe_3O_4@ZnO nanocomposite.

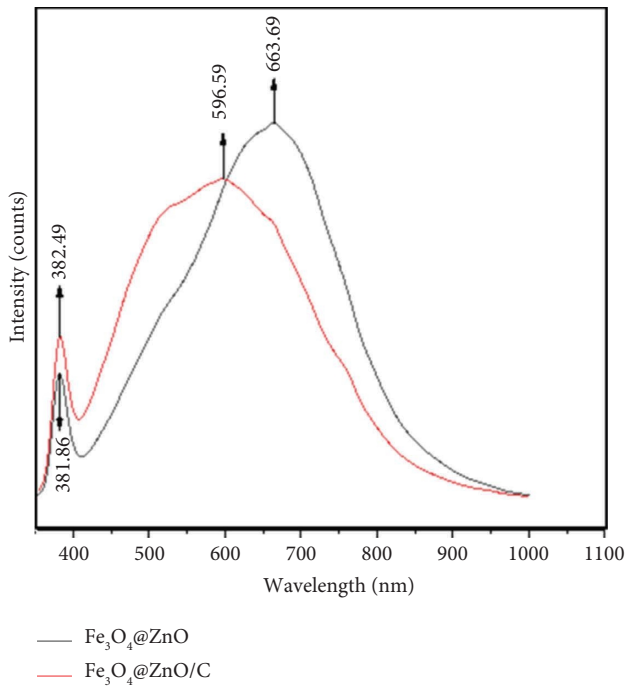

Figure 5: Photoluminescence spectra of the Fe_3O_4@ZnO and Fe_3O_4@ZnO/C nanocomposites.

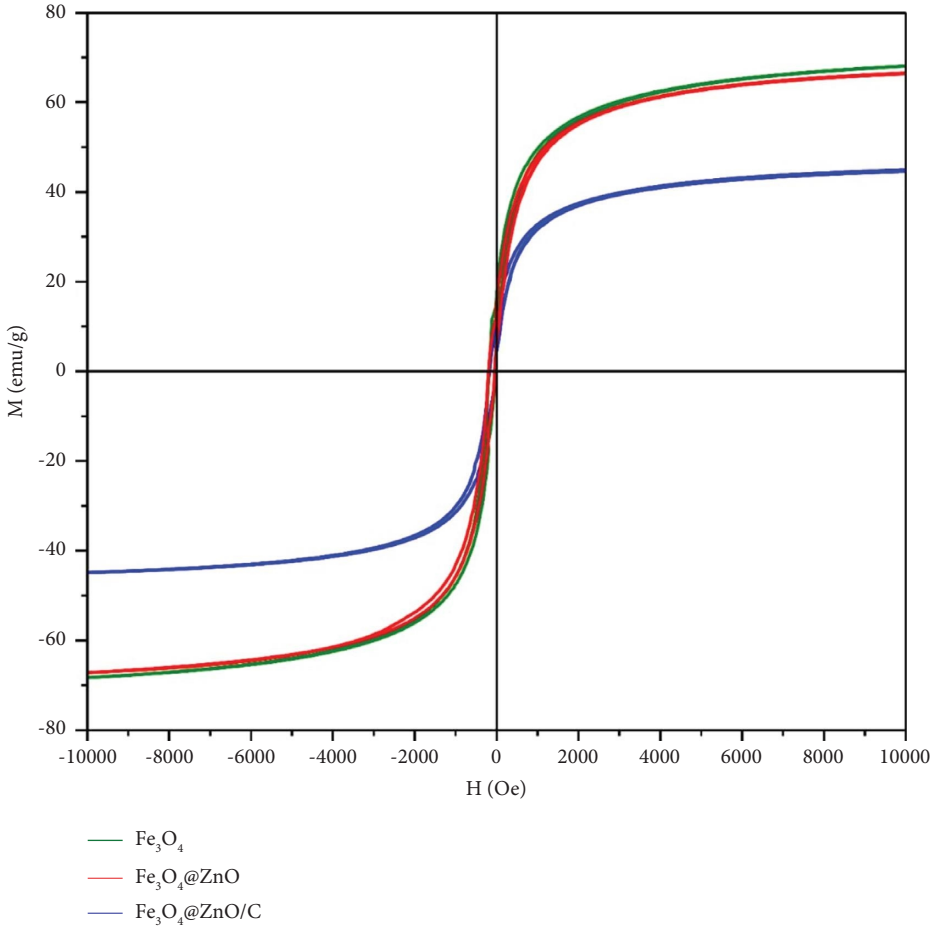

Figure 6: VSM measurement of Fe_3O_4 and nanocomposites.

Table 1: Magnetic properties of Fe_3O_4 and nanocomposites.

Sample	Magnetic properties	
	M_s (emu/g)	H_c (T)
Fe_3O_4	68.10	0.0031
Fe_3O_4@ZnO	66.53	0.0037
Fe_3O_4@ZnO/C	44.65	0.0038

nanoparticles which could reduce the amount of magnetic moment in the sample. The addition of carbon to the sample Fe_3O_4@ZnO caused a decrease in M_s to 44.65 emu/g. This was followed by a slight increase in the value of the coercivity field due to the presence of ZnO and C around Fe_3O_4. The three samples had high magnetic saturation values and low Hc, close to zero. So, these three materials are classified as superparamagnetic. The magnetic saturation value decreases in direct proportion to particle size. The smaller the particle size, the lower the crystallinity. Therefore, reduced crystallinity decreases magnetic saturation [29]. TEM investigation indicates that the particle size of the Fe_3O_4@ZnO/C nanocomposite was smaller than that of the Fe_3O_4@ZnO nanocomposite. Smaller particles caused Fe_3O_4@ZnO/C nanocomposite to have a lower magnetic saturation. However, the decrease in magnetic saturation in the Fe_3O_4@ZnO/C sample was still within the proper range for biomedical applications.

4. Conclusion

The Fe_3O_4@ZnO nanocomposite has a cubic and a hexagonal wurtzite structure for Fe_3O_4 and ZnO, respectively. The addition of carbon increases the absorption of Fe_3O_4@ZnO UV emission. It also broadens and shifts the visible emission to shorter wavelengths. Based on the VSM results, it can be

concluded that there is a decrease in magnetic saturation of the Fe_3O_4@ZnO/C sample which is associated with a reduction of particle size based on TEM results. The presence of carbon also causes a change in photon energy into thermal energy. The addition of carbon to the Fe_3O_4@ZnO nanocomposite increases its biocompatibility as well. However, this does not significantly affect the photoluminescent and magnetic properties of the Fe_3O_4@ZnO/C nanocomposite. Therefore, these materials have the potential to be further developed as biological application materials, especially as bioimaging and photothermal therapy materials.

Data Availability

The data used to support the findings of the study are included within the article.

Conflicts of Interest

The authors declare that they have no conflicts of interest.

Acknowledgments

This research was financially supported by the RKAT FMIPA, Andalas University, with research contract number: 30/UN.16.03.D/PP/FMIPA/2022.

References

[1] H. Nguyen, E. Tinet, T. Chauveau et al., "Bimodal fucoidan-coated zinc oxide/iron oxide-based nanoparticles for the imaging of atherothrombosis," *Molecules*, vol. 24, no. 5, p. 962, 2019.

[2] M. Wu, D. Zhang, Y. Zeng, L. Wu, X. Liu, and J. Liu, "Nanocluster of superparamagnetic iron oxide nanoparticles coated with poly (dopamine) for magnetic field-targeting, highly sensitive MRI, and photothermal cancer therapy," *Nanotechnology*, vol. 26, no. 11, Article ID 115102, 2015.

[3] C. Xiang, X. Zhong, W. Yang et al., "Fe_3O_4 nanoparticles functionalized with polymer ligand for T1-weighted MRI in vitro and in vivo," *Polymers*, vol. 11, no. 5, p. 882, 2019.

[4] G. Kandasamy and D. Maity, "Recent advances in superparamagnetic iron oxide nanoparticles (SPIONs) for in vitro and in vivo cancer nanotheranostics," *International Journal of Pharmaceutics*, vol. 496, no. 2, pp. 191–218, 2015.

[5] J. Pellico, C. M. Ellis, and J. J. Davis, "Nanoparticle-Based Paramagnetic Contrast Agents for Magnetic Resonance Imaging," *Contrast Media & Molecular Imaging*, vol. 2019, Article ID 1845637, 13 pages, 2019.

[6] W. Al Zoubi, A. W. Allaf, B. Assfour, Y. G. Ko, and Y. Ko, "Toward two-dimensional hybrid organic-inorganic materials based on A I-pe/UHV-pvd system for exceptional corrosion protection," *Applied Materials Today*, vol. 24, Article ID 101142, 2021.

[7] V. Zavisova, M. Koneracka, J. Kovac et al., "The cytotoxicity of iron oxide nanoparticles with different modifications evaluated in vitro," *Journal of Magnetism and Magnetic Materials*, vol. 380, pp. 85–89, 2015.

[8] S. Rana, N. G. Shetake, K. C. Barick, B. N. Pandey, H. G. Salunke, and P. A. Hassan, "Folic acid conjugated Fe_3O_4 magnetic nanoparticles for targeted delivery of doxorubicin," *Dalton Transactions*, vol. 45, no. 43, p. 17408, Article ID 17401, 2016.

[9] L. Ding, R. Wang, Y. Hu et al., "Folic acid-modified Laponite®-stabilized Fe_3O_4 nanoparticles for targeted T-weighted MR imaging of tumor," *Applied Clay Science*, vol. 186, Article ID 105447, 2020.

[10] A. Maximenko, J. Depciuch, N. Łopuszyńska et al., "Fe_3O_4@SiO_2@Au nanoparticles for MRI-guided chemo/NIR photothermal therapy of cancer cells," *RSC Advances*, vol. 10, no. 44, p. 26520, Article ID 26508, 2020.

[11] V. M. Thanh, N. T. Huong, D. T. Nam, N. D. T. Dung, L. V. Thu, and M. T. Nguyen-Le, "Synthesis of ternary Fe_3O_4/ZnO/chitosan magnetic nanoparticles via an ultrasound-assisted coprecipitation process for antibacterial applications," *Journal of Nanomaterials*, vol. 2020, Article ID 8875471, 9 pages, 2020.

[12] B. K. Gupta, S. Singh, P. Kumar et al., "Bifunctional luminomagnetic rare-earth nanorods for high-contrast bioimaging nanoprobes," *Scientific Reports*, vol. 6, no. 1, Article ID 32401, 2016.

[13] X. Zhao, Q. Yu, J. Yuan, N. V. Thakor, and M. C. Tan, "Biodegradable rare earth fluorochloride nanocrystals for phototheranostics," *RSC Advances*, vol. 10, no. 26, p. 15393, Article ID 15387, 2020.

[14] R. Gonzalez-Rodriguez, E. Campbell, and A. Naumov, "Multifunctional graphene oxide/iron oxide nanoparticles for magnetic targeted drug delivery dual magnetic resonance/fluorescence imaging and cancer sensing," *PLoS One*, vol. 14, no. 6, Article ID 217072, 2019.

[15] I. Perelshtein, N. Perkas, S. Rahimipour, and A. Gedanken, "Bifunctional carbon dots—magnetic and fluorescent hybrid nanoparticles for diagnostic applications," *Nanomaterials*, vol. 10, no. 7, p. 1384, 2020.

[16] A. Manikandan, E. Manikandan, B. Meenatchi et al., "Rare earth element (REE) lanthanum doped zinc oxide (La: ZnO) nanomaterials: synthesis structural optical and antibacterial studies," *Journal of Alloys and Compounds*, vol. 723, pp. 1155–1161, 2017.

[17] J. Gupta, P. A. Hassan, and K. C. Barick, "Core-shell Fe_3O_4 @ZnO nanoparticles for magnetic hyperthermia and bioimaging applications," *AIP Advances*, vol. 11, no. 2, Article ID 25207, 2021.

[18] S. Abbasi, F. Ahmadpoor, M. Imani, and M.-S. Ekrami-Kakhki, "Synthesis of magnetic Fe_3O_4 @ZnO@graphene oxide nanocomposite for photodegradation of organic dye pollutant," *International Journal of Environmental Analytical Chemistry*, vol. 100, no. 2, pp. 225–240, 2020.

[19] H. Qiu, B. Cui, G. Li et al., "Novel Fe_3O_4 @ZnO@mSiO_2 nanocarrier for targeted drug delivery and controllable release with microwave irradiation," *Journal of Physical Chemistry C*, vol. 118, no. 27, p. 14937, Article ID 14929, 2014.

[20] C. Wang, L. Zhang, S. Li et al., "A designed synthesis of multifunctional Fe_3O_4 @carbon/zinc phosphate nanoparticles for simultaneous imaging and synergic chemo-photothermal cancer therapy," *Journal of Materials Chemistry B*, vol. 4, no. 35, pp. 5809–5813, 2016.

[21] M. Stepanova, A. Dubavik, A. Efimova et al., "Magneto-luminescent nanocomposites based on carbon dots and ferrite with potential for bioapplication," *Nanomaterials*, vol. 12, no. 9, p. 1396, 2022.

[22] N. Dizge, Y. Ozay, U. B. Simsek et al., "Preparation, characterization and comparison of antibacterial property of polyethersulfone composite membrane containing zerovalent iron or magnetite nanoparticles," *Membrane Water Treatment*, vol. 8, no. 1, pp. 51–71, 2017.

[23] M. Nikazar, M. Alizadeh, R. Lalavi, and M. H. Rostami, "The optimum conditions for synthesis of Fe_3O_4/ZnO core/shell magnetic nanoparticles for photodegradation of phenol," *Journal of Environmental Health Science and Engineering*, vol. 12, no. 1, p. 21, 2014.

[24] Astuti, S. Arief, M. Muldarisnur, Zulhadjri, and S. R. A. Usna, "Enhancement in photoluminescence performance of carbon-based Fe_3O_4@ZnO–C nanocomposites," *Vacuum*, vol. 211, Article ID 111935, 2023.

[25] H. Nurul Ulya, A. Taufiq, and Sunaryono, "Comparative structural properties of nanosized zno/fe_3o_4 composites prepared by sonochemical and sol-gel methods," *IOP Conference Series: Earth and Environmental Science*, vol. 276, no. 1, Article ID 12059, 2019.

[26] V. Madhubala and T. Kalaivani, "Phyto and hydrothermal synthesis of Fe_3O_4@ZnO core-shell nanoparticles using Azadirachta indica and its cytotoxicity studies," *Applied Surface Science*, vol. 449, pp. 584–590, 2018.

[27] M. Willander, O. Nur, J. R. Sadaf et al., "Luminescence from zinc oxide nanostructures and polymers and their hybrid devices," *Materials*, vol. 3, no. 4, pp. 2643–2667, 2010.

[28] Z. M. Liao, H. Z. Zhang, Y. B. Zhou, J. Xu, J. M. Zhang, and D. P. Yu, "Surface effects on photoluminescence of single ZnO nanowires," *Physics Letters A*, vol. 372, no. 24, pp. 4505–4509, 2008.

[29] M. R. Ghazanfari, M. Kashefi, S. F. Shams, and M. R. Jaafari, "Perspective of Fe_3O_4 nanoparticles role in biomedical applications," *Biochemistry Research International*, vol. 2016, Article ID 7840161, 32 pages, 2016.